Since January 2020 Elsevier has created a COVID-19 resource centre with free information in English and Mandarin on the novel coronavirus COVID-19. The COVID-19 resource centre is hosted on Elsevier Connect, the company's public news and information website.

Microchemical Journal 190 (2023) 108696

Contents lists available at ScienceDirect

Microchemical Journal

journal homepage: www.elsevier.com/locate/microc

Synergistic effect of gold nanoparticles anchored on conductive carbon black as an efficient electrochemical sensor for sensitive detection of anti-COVID-19 drug Favipiravir in absence and presence of co-administered drug Paracetamol

Rasha M.K. Mohamed [a,*], Sabrein H. Mohamed [a], Aml M. Asran [a], Ibrahim H. Alsohaimi [a], Hassan M.A. Hassan [a], Hossieny Ibrahim [b,*], Mohamed M. El-Wekil [c]

[a] Department of Chemistry, College of Science, Jouf University, P.O. Box 2014, Sakaka, Saudi Arabia
[b] Department of Chemistry, Faculty of Science, Assiut University, Assiut 71516, Egypt
[c] Department of Pharmaceutical Analytical Chemistry, Faculty of Pharmacy, Assiut University, Assiut 71526, Egypt

ARTICLE INFO

Keywords:
Favipiravir
Paracetamol
Electrochemical sensor
Simultaneous
Antiviral

ABSTRACT

Favipiravir (FVP) is introduced as a promising newly developed antiviral drug against the coronavirus disease 2019 (COVID-19). Therefore, the accurate determination of FVP is of great significance for quality assessment and clinical diagnosis. Herein, a novel electrochemical sensing platform for FVP based on gold nanoparticles anchored conductive carbon black (Au@CCB) modified graphite nanopowder flakes paste electrode (GNFPE) was constructed. Morphological and nanostructure properties of Au@CCB have been investigated by TEM, HRTEM, and EDX methods. The morphology and electrochemical properties of Au@CCB/GNFPE were characterized by SEM, cyclic voltammetry (CV), and EIS. The Au@CCB nanostructured modified GNFPE exhibited strong electrocatalytic ability towards the oxidation of FVP. The performance of the fabricated Au@CCB/GNFPE was examined by monitoring FVP concentrations in the absence and presence of co-administered drug paracetamol (PCT) by AdS-SWV. It was demonstrated that the proposed sensor exhibited superior sensitivity, stability, and anti-interference capability for the detection of FVP. The simultaneous determination of a binary mixture containing FVP and the co-administered drug PCT using Au@CCB/GNFPE sensor is reported for the first time. Under optimized conditions, the developed sensor exhibited sensitive voltammetric responses to FVP and PCT with low detection limits of 7.5 nM and 4.3 nM, respectively. The sensing electrode was successfully used to determine FVP and PCT simultaneously in spiked human plasma and pharmaceutical preparations, and the findings were satisfactory. Finally, the fabricated sensor exhibited high sensitivity for simultaneous detection of FVP and PCT in the presence of ascorbic acid in a real sample.

1. Introduction

The appearance of the COVID-19 caused by the SARS-CoV-2 virus was crucial for our global society, causing a widespread pandemic with devastating health, social, and economic challenges for communities worldwide. This pandemic has prompted researchers to produce medications or vaccines to reduce or stop the progression and spread of this disease. One of the primary treatment methods is to use antiviral drugs such as favipiravir (FVP, Scheme 1), which is approved for influenza treatment and is currently considered in the treatment of COVID-19 [1,2]. The dosage regimen of FVP plays an important role in COVID-19 treatment, as inappropriate dosage may lead to subtherapeutic or toxic concentrations without clear clinical benefit. Therefore, the widespread use of FVP for COVID-19 treatment with maximum therapeutic effects and minimum toxicities necessitates developing an accurate, sensitive, and fast technique for detecting FVP in real samples to avoid its deleterious side effects and control its concentration [3].

Favipiravir can be determined by a variety of analytical methods. Spectrofluorometry [4,5], high-performance liquid chromatography (HPLC) [6], fluorescence [7], TLC [8] and liquid chromatography-tandem mass spectrometry (LC–MS/MS) [9] have been utilized. Most of these techniques may require expensive equipment, long analysis

* Corresponding authors.
E-mail addresses: rmabdelbaky@ju.edu.sa (R.M.K. Mohamed), Hossieny.Ibrahim@aun.edu.eg (H. Ibrahim).

https://doi.org/10.1016/j.microc.2023.108696
Received 26 January 2023; Received in revised form 15 March 2023; Accepted 27 March 2023
Available online 31 March 2023

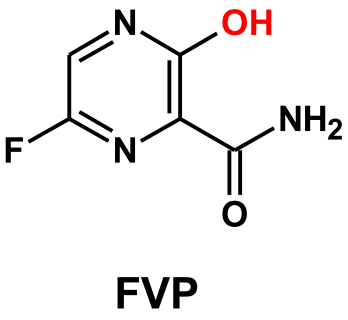

Scheme 1. Chemical structure of Favipiravir (FVP).

time, tedious sample preparation, and technical expertise. Therefore, a selective and sensitive sensor is required to determine FVP in pharmaceutical and biological samples such as urine and plasma. As a practical alternative strategy, the electrochemical analysis methods have the advantages of simple fabrication, convenient operation, fast response, cost effectiveness, and remarkable sensitivity [10–16]. However, the electrochemical methods also suffer from a high selectivity in detecting analytes. To tackle this issue, using appropriate nanomaterials on electrodes is a novel strategy to increase the developed electrode's selectivity and active surface area.

Nanomaterials have recently emerged as one of the most fascinating fields of science and nanotechnology. Several electrochemical sensing platforms make use of nanomaterials like nanocomposite, metal nanoparticles, and carbon nanomaterials [17–21]. Conductive carbon black (CCB) is a category of carbon nanomaterial with a large surface area and provide a charge transporting pathway to the electrode. CCB modified electrodes (CCBME) exhibit unique electrochemical and electronic properties and are widely used in electrochemical sensing applications owing to their good conductivity, low toxicity, biocompatibility and low cost nanomaterial [22–24]. However, the electrochemical performance of CCBME is extremely dependent on adequate sensing surface modification [25–27]. In the development of electrochemical sensors, gold nanoparticles (AuNPs) have received considerable interest due to its advantages of simple preparation, excellent electro-catalytic ability, a large specific surface area, and excellent biocompatibility [28–30].

In this study, AuNPs anchored on the surface of CCB (Au@CCB) nanocomposite was prepared. Then, the nanostructured Au@CCB was used to modify the surface of graphite nanopowder flakes paste electrode (GNFPE) to develop a novel electrochemical sensor (Au@CCB/GNFPE) with high performance because hybrid nanomaterials could provide larger electrochemically active surface areas for the adsorption of FVP and effectively accelerate the electron transfer. Benefiting from the synergistic effect between AuNPs and CCB, this sensor possessed high selectivity and accuracy for the detection of the antiviral drug FVP. Interestingly, Au@CCB/GNFPE exhibit high electrocatalytic activity, high sensitivity, excellent stability, and reproducibility for the determination of FVP.

Moreover, no efforts have been devoted to the determination of FVP in the presence of the co-administered drug paracetamol (PCT) in pharmaceutical formulations or human plasma samples. The infection with COVID-19 causes several symptoms and requires either "add-on" treatment medication such as pain-relief drug PCT [31]. Therefore, it is of prime importance to evaluate the performance of the proposed sensor for the simultaneous determination of FVP and PCT that may result in drug-drug interactions through the course of COVID-19 treatment. According to our knowledge, no electrochemical approaches were reported for the simultaneous detection of FVP and PCT utilizing Au@CCB nanocomposite modified GNFPE in pure form, spiked human plasma, and dosage form (Scheme 2). Finally, the practical performance of the sensing electrode was evaluated by the simultaneous detection of FVP and PCT in the presence of AA in human plasma samples.

2. Experimental

2.1. Materials, reagents and instruments

Materials, reagents, instruments, and preparation of real samples are presented in Electronic Supplementary Materials (ESM).

2.2. Synthesis of Au@CCB nanocomposite

Firstly, the CCB were purified with acid treatment as described elsewhere [32]. Next, Au@CCB nanocomposite was synthesized by reduction of $HAuCl_4$ with sodium citrate solution according to previous work [33]. Briefly, 1.5 g of purified CCB were dispersed in $HAuCl_4$ solution (100 mL, 0.25 mM). The resulting dispersion was boiled and stirred vigorously, then 2% (w/v) trisodium citrate was added. The resultant black residue was washed successively with deionized water. The washed product was dried at 60 °C for 10 h to obtain the final Au@CCB nanocomposite.

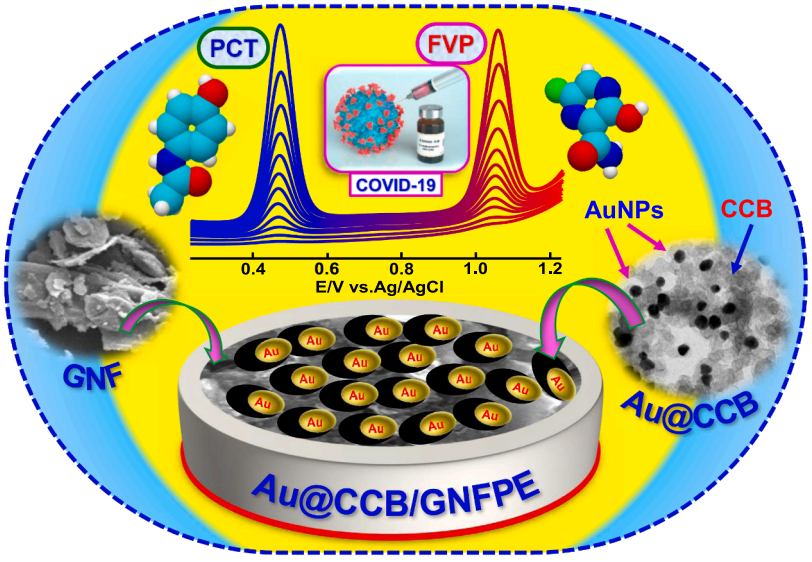

Scheme 2. Development of the modified sensor for simultaneous determination of FVP and PCT.

2.3. Construction of the electrodes

The bare graphite paste electrode (GPE) and graphite nanopowder flakes paste electrode (GNFPE) were prepared by mixing paraffin oil and graphite powder or graphite nanopowder flakes (GNF) in an agate mortar (80:20 w/w). The resultant mixture was filled into a 3 mm diameter Teflon cavity (Geometric area; $A_G = 0.07\ cm^2$). The Au@CCB nanocomposite modified GNFPEs (Au@CCB/GNFPEs) were prepared by mixing (5, 10, 15, 20, and 25% w/w) of Au@CCB with GNF and 20% of paraffin oil. For comparison, CCB/GNFPE was fabricated with similar procedures.

3. Results and discussion

3.1. Structural and Morphological investigation

The XRD patterns of the CCB and Au@CCB nanocomposite were presented in Fig. S1A (ESM).

The morphology of CCB and the prepared Au@CCB nanocomposite was characterized by TEM, HR-TEM, and EDX. Fig. 1A shows CCB nanomaterials with spheres (40–60 nm) that have a rough surface and exist in the form of aggregates. After modification (Fig. 1B), the AuNPs were evenly distributed and presented as a uniform sphere anchored on CCB. Fig. 1C displays the d-spacing value of 0.22 nm, confirming the (1 1 1) crystal phase of Au. To confirm the presence of AuNPs atoms on the CCB, EDX analysis was carried out. Apparent signature peaks of Au were displayed, which showed the effective surface coverage of the Au nanoparticles on CCB (Fig. S1B). The size distribution histogram (Fig. S1B, inset) was obtained from HRTEM, and it was observed that the particle size of AuNPs was 21.5 ± 0.7 nm. Furthermore, EDX-mapping of Au@CCB revealed that gold nanoparticles and carbon are the major elements (Fig. S1C).

The morphology analysis of GNFPE and Au@CCB/GNFPE was performed by SEM examination. The surface of the GNFPE was composed of flakes with large gaps between the graphite nanopowder flakes (Fig. 1D). The SEM image of the Au@CCB/GNFPE (Fig. 1E&F) shows that smaller particles of Au@CCB nanocomposite are well dispersed into the large gaps between the graphite nanopowder flakes, which results in a higher conductivity.

3.2. Electrochemical properties of sensing electrodes

The charge transfer capacity of the bare and modified electrodes was evaluated by using EIS executed in 0.1 M potassium chloride with a probe of 5.0 mM $[Fe(CN)_6]^{3-/4-}$. Fig. 2A shows the EIS Nyquist plots of GPE, GNFPE, CCB/GNFPE, and Au@CCB/GNFPE. As can be seen, the charge transfer resistance (R_{ct}) value (1930 ± 38 Ω, RSD = 2.0%) of the GPE is significantly high due to the large-size of the graphite flakes, which cause the poor conductivity of the GPE [34]. In the case of GNFPE, the R_{ct} value relatively decreases (1740 ± 28 Ω, RSD = 1.6%), which is due to the smaller particle size of graphite nanopowder flakes. After modification, the R_{ct} value of CCB-GNFPE was 700 ± 16 Ω (RSD = 2.3%), indicating that the CCB improved interfacial electron transferability. Interestingly, the Au@CCB/GNFPE produced R_{ct} of 300 ± 5 Ω (RSD = 1.7%), which is 6.4, 5.8, and 2.3 times lower than the R_{ct} at the GPE, GNFPE, and CCB/GNFPE, respectively. These results demonstrated that the Au@CCB nanocomposite can be an effective platform that enhances charge transfer process and improves electrode conductivity.

Additionally, the charge transfer resistance (R_{ct}) can be used to evaluate the heterogeneous rate constant (k_{et}) and the standard exchange current density (I_0) over the fabricated electrodes using Eqs. (1 and 2) [35,36]:

$$k_{et} = RT / F^2 R_{ct} A C \quad (1)$$

$$I_o = RT / n F R_{ct} \quad (2)$$

where C is the concentration of Fe^{2+}/Fe^{3+} system, F = 96485 C mol^{-1}, R = 8.314 J K^{-1} mol^{-1} and T is the temperature. At the bare GPE, a low k_{et} of 3.9 × 10^{-4} cm s^{-1} was produced, indicating poor conductivity. However, when Au@CCB was incorporated with GNFPE (Au@CCB/GNFPE), a significant increase in k_{et} (2.5 × 10^{-3} cm s^{-1}) was observed, confirming the synergetic impact of Au nanoparticles and CCB. Moreover, the I_0 value obtained for the Au@CCB/GNFPE increases, which is almost a 5.7-fold elevation when compared with GPE (Table 1). The obtained results indicate that the Au@CCB/GNFPE sensor has faster electron transfer properties and better electro-catalytic activity than the others.

To investigate the electrochemical properties of synthesized Au@CCB nanocomposite, CV studies have been carried out in a solution

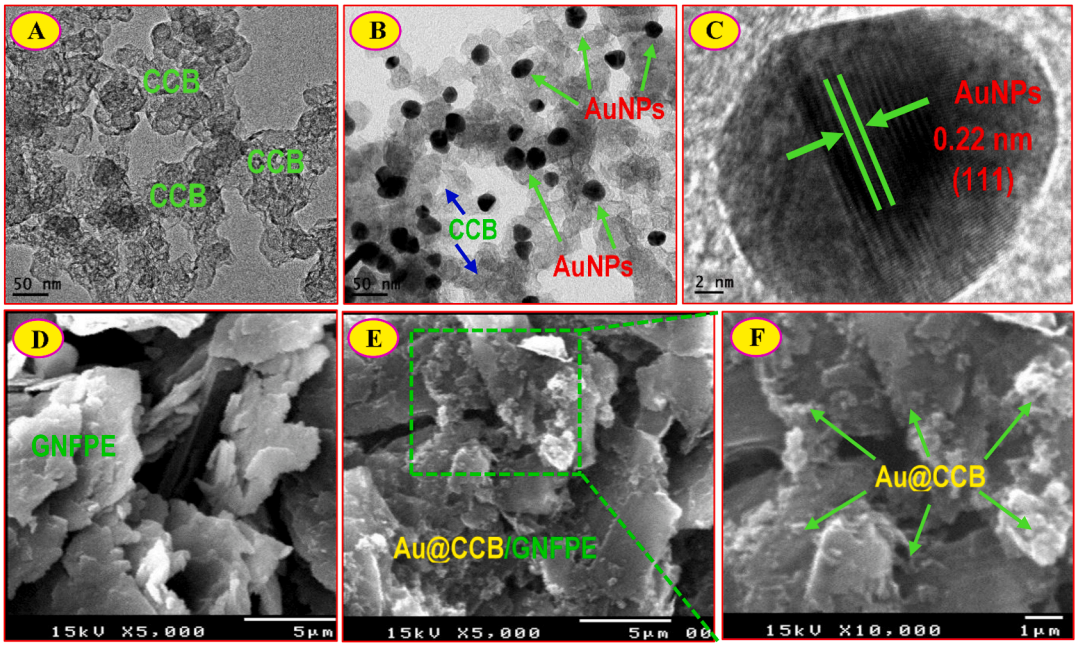

Fig. 1. TEM images of CCB (A), Au@CCB (B), HRTEM micrograph of AuNPs showing the inter-planar spacing (C), SEM images of GNFPE (D) and Au@CCB/GNFPE (E, F).

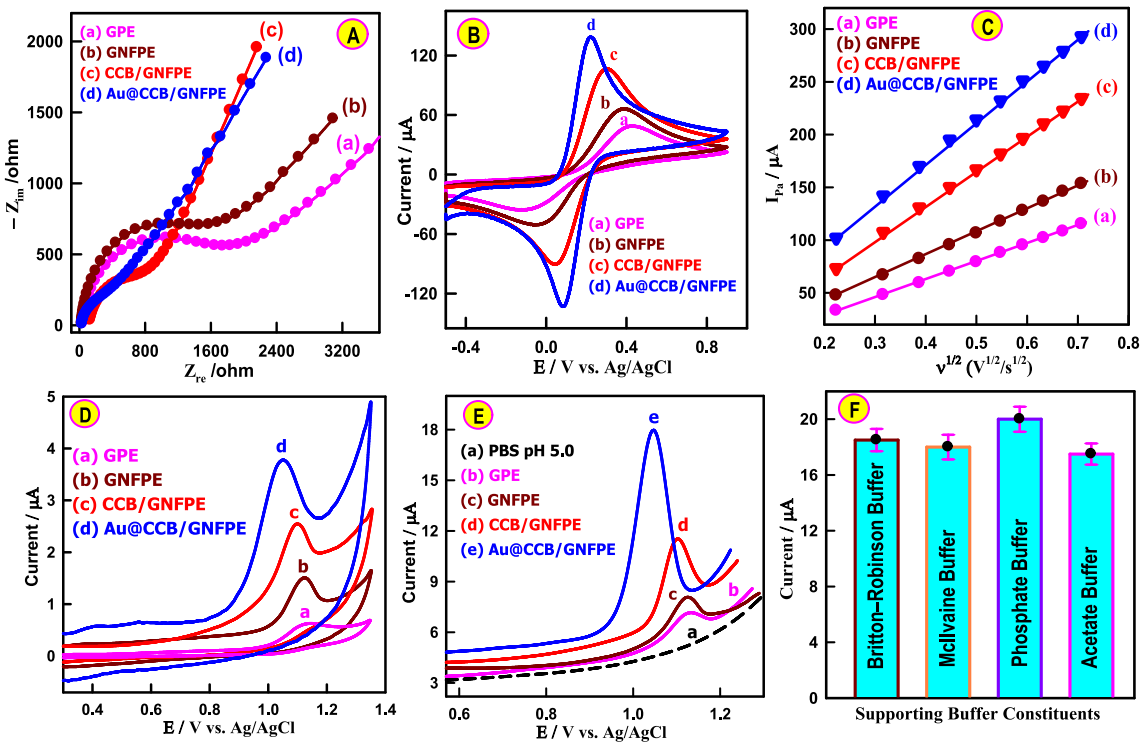

Fig. 2. (A) Nyquist plots and (B) CVs of (a) GPE, (b) GNFPE, (c) CCB/GNFPE and (d) Au@CCB/GNFPE in 5 mM $[Fe(CN)6]^{3-}$/ $[Fe(CN)_6]^{4-}$ (1:1 mixture) solution containing 0.1 M KCl at a scan rate of 100 mVs^{-1}. (C) Plot of I_{Pa} vs. $\nu^{½}$. (D) CVs of 7.5 µM FVP in PB solution of pH 5.0 obtained (a) GPE, (b) GNFPE, (c) CCB/GNFPE and (d) Au@CCB/GNFPE. (E) AdS-SW voltammograms of 24.0 µM FVP on the surface of (a) GPE, (b) GNFPE, (c) CCB/GNFPE and (d) Au@CCB/GNFPE in PB solution of pH 5.0. (F) The bar diagram exhibits the different supporting buffer constituents versus anodic peak current response of 24.0 µM FVP.

Table 1
Electrochemical data of 5 mM $[Fe(CN)_6]^{-3/-4}$ in 0.1 M KCl at different working electrodes.

Electrodes	From EIS			From CV			
	R_{ct} (Ω)	k_{et} × 10^{-4} (cm s^{-1})	I_o (µA cm^{-1})	ΔE_P (mV)	I_{Pa} (µA)	A_{eff} (cm^2)	R_f
GPE	1930 ± 38[a]	3.9	13	521	51	0.15 ± 0.005[a]	2.0
GNFPE	1740 ± 28	4.5	15	416	68	0.20 ± 0.008	2.7
CCB/ GNFPE	700 ± 16	11	37	251	109	0.28 ± 0.012	4.0
Au@CCB/ GNFPE	300 ± 5	25	86	137	141	0.40 ± 0.014	5.7

R_{ct}, charge transfer resistance; k_{et}, the heterogeneous electron transfer rate constant; I_o, standard exchange current density; A_{eff}, effective surface area (cm^2); R_f, roughness factor.
[a] Mean ± Standard deviation for n = 3.

of 0.1 M potassium chloride with a probe of 5.0 mM $[Fe(CN)_6]^{3-/4-}$. Fig. 2B shows the CV response for GPE, GNFPE, CCB/GNFPE, and Au@CCB/GNFPE recorded at the scan rate of 100 mV/s. We observe an increase in anodic current (I_{Pa}) and a decrease of a peak potential separation (ΔE_P) in the order of bare GPE < GNFPE < CCB/GNFPE < Au@CCB/GNFPE (Table 1). The results showed that the Au@CCB nanocomposite had a large surface-to-volume ratio and excellent conductivity, which promoted electron transfer at the electrochemical interface.

The electrochemically effective surface area (A_{eff}, cm^2) of the fabricated electrodes is estimated using the Randles-Sevcik Eq. (3) [37]:

$$I_{Pa} = (2.69 \times 10^5)\, n^{3/2} A_{eff} D^{1/2} \nu^{1/2} C \quad (3)$$

The CV measurements of the suggested electrodes were recorded at different scan speeds in a solution of 0.1 M potassium chloride with a probe of 5.0 mM $[Fe(CN)_6]^{3-/4-}$ (Fig. S2). The A_{eff} values were estimated using I_{Pa} vs. $\nu^{1/2}$ plots (Fig. 2C). The results showed that the A_{eff} of Au@CCB/GNFPE (0.40 ± 0.014) was greater than bare GPE (0.15 ± 0.005), GNFPE (0.20 ± 0.008), and CCB/GNFPE (0.28 ± 0.012) (Table 1). A significant increase in A_{eff} of Au@CCB/GNFPE, which confirmed the synergistic impact of Au nanoparticles and CCB in the Au@CCB nanocomposite. Furthermore, the surface roughness factor ($R_f = A_{eff}/A_G$) evaluated for Au@CCB/GNFPE ($R_f = 5.7$) is greater than the GPE ($R_f = 2.0$), GNFPE ($R_f = 2.7$) and CCB/GNFPE ($R_f = 4.0$). Based on these results, further electro-catalytic studies have been made on Au@CCB/GNFPE sensor.

3.3. Electro-catalytic oxidation of FVP at Au@CCB/GNFPE sensor

The CV and AdS-SWV techniques were used to examine the electro-catalytic oxidation of FVP at the Au@CCB/GNFPE sensor. Fig. 2D shows cyclic voltammograms recorded in the presence of 7.5 µM of FVP at 100 mV/s sweep rate. The oxidative irreversible response of FVP at the Au@CCB/GNFPE was larger (I_{Pa} = 3.1 µA, curve d) than that at the bare GPE (I_{Pa} = 0.5 µA, curve a), and the E_{Pa} was shifted negatively to + 1.05 V. This behavior suggested that the electro-catalytic ability of the Au@CCB/GNFPE sensor toward FVP oxidation was better due to the enhanced electroactive surface area of the Au@CCB nanocomposite, which provides more favorable adsorption sites and catalytic oxidation of FVP.

AdS-SWV is the most commonly used technique for organic compound measurement because it can accurately determine substances at very low trace concentrations. As shown in Fig. 2E, the electro-catalytic oxidation of FVP yielded higher current and occurred at a lower E_{Pa} at the Au@CCB/GNFPE (I_{Pa} = 11.0 µA, E_{Pa}= +1.05 V) in comparison to bare GPE (I_{Pa} = 1.2 µA, E_{Pa} = 1.14 V). All these results confirm that the

Au@CCB/GNFPE acts as a good electro-catalyst for sensing the target analyte FVP, and this electrode is used for further studies.

3.4. The influence of pH and supporting electrolyte

The electro-catalytic oxidation of FVP in PB solution with different pH ranging from 3 to 8 at Au@CCB/GNFPE was measured by AdS-SWV (Fig. S3A). The current response increased as the pH value increased from 3.0 to 5.0 and then decreased with the increasing pH value. Therefore, we chose the pH value of the FVP solution at 5.0 as the best detection condition for further measurements. The peak potential showed a negative shift as pH was increased from 3.0 to 8.0 and exhibited a good linear relationship with pH (Fig. S3B). The regression equation was E_{Pa} (V) = 1.3 – 0.054 pH, R^2 = 0.9993. This slope of the plot between E_{Pa} (V) and pH implied that equal numbers of electrons and protons were involved in the electro-catalytic oxidation of FVP on the Au@CCB/GNFPE sensor [12,13].

The supporting solution is one of the key elements affecting the behaviour of the constructed sensor. Therefore, the AdS-SWV responses of 24 μM FVP at the Au@CCB/GNFPE sensor were monitored in various supporting electrolytes (Fig. 2F). Among all the supporting electrolytes, a maximum current response was monitored for FVP in PB solution at pH 5.0.

3.5. Optimization of Au@CCB nanocomposite in the Au@CCB/GNFPE

The incorporation of Au@CCB nanostructure into the Au@CCB/GNFPE sensor composition can affect the performance of the developed sensor. Fig. S3C shows the current responses of different amounts of Au@CCB nanocomposite (5, 10, 15, 20, and 25% w/w of Au@CCB to graphite nanopowder flakes) in PB solution containing FVP. The anodic current response increased with increments of Au@CCB from 5.0% to 15.0%, and decreased gradually with further increments. The larger effective surface area of the Au@CCB nanocomposite provided more catalytic and adsorption sites, producing a high current response. Therefore, 15.0% was the most suitable amount of Au@CCB for the construction of Au@CCB/GNFPE sensor to detect FVP.

3.6. The impact of sweep rate

The influence of scan rate on the electrochemical oxidation of 7.5 μM FVP at the Au@CCB/GNFPE was investigated by CV, scanning from 50 to 600 mVs^{-1} (Fig. S4A). The increase in sweep rate resulted in an enhancement of the oxidation peak current, and the peak potential shifted towards the positive direction. This behavior indicated the irreversibility of FVP oxidation at the proposed sensor. Fig. S4B exhibits the proportional relationship between I_{Pa} versus the scan rate and observed regression equation as I_{Pa}(μA) = 0.6 + 0.015 ν (mV/s) (R^2 = 0.989). Furthermore, a good linear relationship (Fig. S4C) was observed between the logarithm of scan rate (log ν) and the logarithm of peak current (log I_{Pa}), and the linear slope was equal to 0.87, which was close to the theoretical value 1.0 of the pure adsorption process [38]. Additionally, the number of electrons transferred from FVP to the surface of the Au@CCB/GNFPE during the electro-catalytic oxidation process was obtained using the slope of the plot of E_{Pa} and ln ν, which produced a linear equation expressed as: E_{Pa} (V) = 1.1 + 0.028 Ln ν (R^2 = 0.989) (Fig. S4D). Based on the slope of the linear plot, which was 0.028, αn was calculated to be 0.92. Using the value of the α = 0.68 obtained from the equation α = (47.7/E_P – $E_{P/2}$) [20], the electron transfer number during the FVP oxidation was 1.35 (≈ 1.0), which is consistent with other reports [12,13]. The proposed mechanism of FVP oxidation catalyzed by the Au@CCB/GNFPE can be described in Scheme 3.

3.7. Sensitive determination of FVP in absence and presence of PCT

Under optimum experimental conditions (Fig. S5), the electrochemical sensing performance of the Au@CCB/GNFPE sensor towards FVP detection in the absence of PCT was measured utilizing the AdS-SWV (Fig. 3A). As shown in Fig. 3A (inset), the fabricated sensor displayed a linear response for FVP from 0.03 to 77.3 μM, and the linear equation was expressed as follows: I_{Pa} (μA) = 0.48 (μM) FVP – 0.6 (R^2 = 0.9972). The limit of detection (LOD) and limit of quantitation (LOQ) of the designed sensor toward FVP were calculated as 8.1 nM and 27.0 nM, respectively, while the sensitivity was estimated to be 6.9 $\mu A \mu M^{-1} cm^{-2}$ (Table 2). The fabricated Au@CCB/GNFPE sensor is compared to the reported FVP systems (Table 3). The proposed sensing platform displayed a wide dynamic range and a lower LOD than most of the published platforms. These results proved that the constructed Au@CCB/GNFPE sensor was quite sensitive, even at very low concentrations.

Electrochemical sensing of FVP at the Au@CCB/GNFPE sensor has been measured at pH 5.0 in the presence of an excess of PCT. Fig. 3B shows the AdS-SW voltammograms of FVP for various concentrations ranging from 0.03 to 76.5 μM while keeping the concentration of PCT constant at 29.0 μM. As presented in Fig. 3B (inset), the peak current of FVP and its concentration exhibited good linearity, and the linear equation was: I_{Pa} (μA) = 0.49 (μM) FVP – 0.57 (R^2 = 0.9971). The LOD, LOQ and sensitivity were calculated to be 7.6 nM, 25.5 nM, and 7.0 $\mu A \mu M^{-1} cm^{-2}$ respectively (Table 2). It is interesting to observe that the sensitivities of the Au@CCB/GNFPE towards FVP in the absence and presence of PCT were virtually the same, which confirms that monitoring these two drugs together by using the fabricated sensor is possible.

3.8. Selectivity, reproducibility, and stability of Au@CCB/GNFPE

The anti-interference performance of Au@CCB/GNFPE was evaluated in the presence of various species that can present in real samples. As presented in Fig. S6, 200-folds of concentration of Na^+, 100-folds of concentrations of Ca^{2+}, Na^+, Mg^{2+}, SO_4^{2-}, Cl^- and NO_3^- and 50-folds concentrations of uric acid (UA), acyclovir (ACV), citric acid (CA), glucose (Glu), dopamine (DA), hydroxychloroquine (HCQ), remdesivir (REM) and microcrystalline cellulose (MCC) did not significantly interfere with the current responses of FVP, and relative errors are less than ± 5%. These results indicated that the proposed sensor has favorable anti-interference for FVP determination.

The repeatability of the detection of FVP using the Au@CCB/GNFPE was measured by monitoring the current response of three FVP concentrations ten times. The relative standard deviations (RSDs) of the

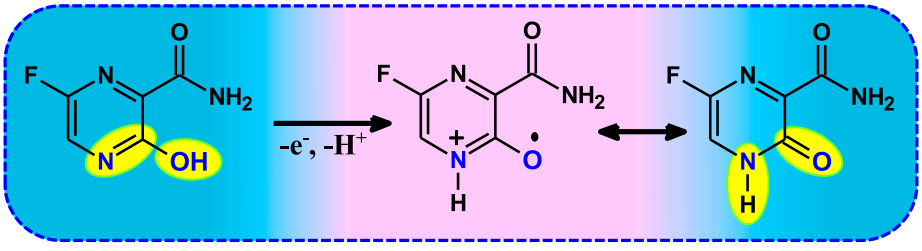

Scheme 3. The proposed electrochemical oxidation mechanism of FVP at Au@CCB/GNFPE sensor.

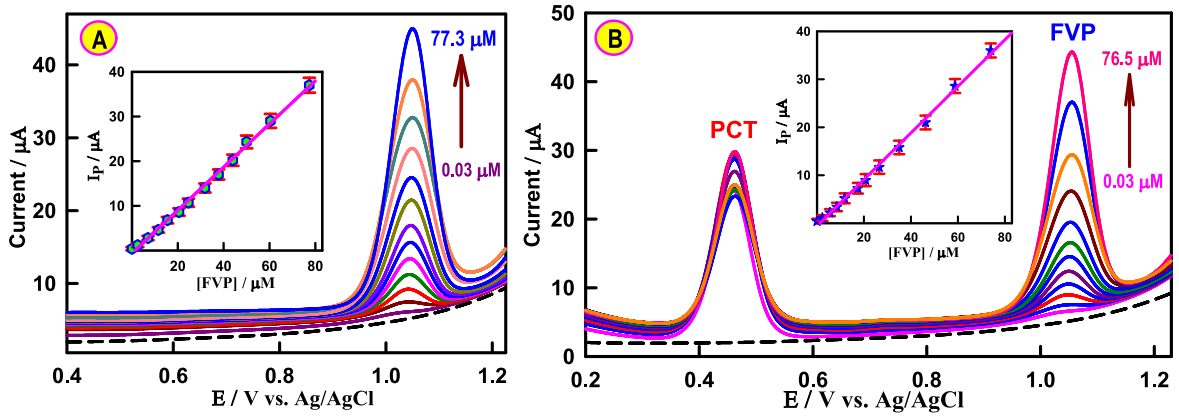

Fig. 3. (A) AdS-SW voltammograms of Au@CCB/GNFPE in the absence (1) and presence of FVP from 0.03 to 77.3 µM in PB solution of pH 5. Inset: calibration plot of I_{Pa}(µA) versus [FVP]/µM. (B) AdS-SW voltammograms of Au@CCB/GNFPE in PB solution pH 5.0 with varied concentrations of FVP (0.03–76.5 µM) in presence of 29.0 µM PCT, Inset: calibration plot of I_{Pa}(µA) versus [FVP]/µM.

Table 2
Regression data of the calibration lines for quantitative determination of FVP in standard solution in absence and presence of PCT at Au@CCB/GNFPE using AdS-SWV.

Parameters	In absence of PCT	In presence of PCT
Linearity range (µM)	0.03 – 77.3	0.03 – 76.5
Slope (µAnM^{-1})	480	490
Standard error of slope	0.008	0.007
Intercept (µA)	−0.6	−0.57
Standard error of intercept	0.28	0.27
Coefficient of determination (R^2)	0.9972	0.9971
Standard error of estimate	0.63	0.64
Number of measurements (n)	3	3
LOD (nM)	8.1	7.6
LOQ (nM)	27	25.5
Sensitivity ($\mu A\ \mu M^{-1}\ cm^{-2}$)	6.9	7.0

Table 3
A comparison of electrodes for the individual determination of FVP and PCT.

Analyte	Electrode	LDR / µM	LOD / nM	Ref.
FVP	CPT-BDD/GCE	0.064 – 130	18.0	[10]
	MnO_2-rGO SPE	0.01 – 55	9.0	[11]
	DNPs/CPE	0.02 – 1.0	4.83	[12]
	GC/MWCNTs + ILCs	0.9 – 150	16.0	[13]
	Pt@rGO/GCE	3.16 – 100	2460	[14]
PCT	AuNPs/ MWCNT/ GCE	0.09 – 35	30	[39]
	PEDOT/GO/GCE	10 – 60	570	[40]
	Pt/NDG	0.05 – 90	8.0	[41]
	GCE/Pd-SB	1.0 – 50	67	[42]
	γ-Fe_2O_3/CNTs	2.5–385	46	[43]
	ZnO/FMWCNT/CPE	0.5 – 13	23	[44]
FVP	Au@CCB/GNFPE	0.03 – 77.3	8.1	This
FVP and PCT	Au@CCB/GNFPE	FVP: 0.03 – 75	7.5	work
		PCT: 0.05 – 50	4.3	

Note: LOD (limit of detection) LDR (linear dynamic range), GCE (glassy carbon electrode), PEDOT (poly(3, 4-ethylenedioxythiophene), GO (graphene oxide), Pt (platinum), NDG (nitrogen doped graphene), Pd-SB (Pd-Schiff base), CPT-BDD GCE (cathodically pretreated boron-doped diamond glassy carbon electrodes), MnO_2-rGO SPE (MnO_2-reduced graphene oxide screen-printing electrodes), DNPs/CPE (diamond nanoparticles/carbon paste electrode), GC/MWCNTs + ILCs (glassy carbon / carbon nanotubes-ionic liquid crystals).

current responses obtained from 2.5, 11.5 and 20.5 µM FVP, respectively, were 3.2%, 2.1% and 1.6% (Fig. 4A). The reproducibility of the construction of the Au@CCB nanocomposite modified GNFPE was evaluated by preparing six sensors at different times (Fig. 4B). The RSD for the seven electrodes was determined to be 1.8%. Moreover, the long-term storage stability was analyzed by AdS-SWV in 11.5 µM FVP using the fabricated electrode for 40 days at room temperature (Fig. 4C). The observed peak current reduced less than 5% (3.2%) of the initial signal after 40 days. These results imply that the fabricated Au@CCB/GNFPE has excellent repeatable measurement, reproducible preparation, and satisfactory stability for the electrochemical detection of FVP.

3.9. Simultaneous determination of FVP and PCT

One of the goals of this work was the detection of FVP and PCT simultaneously. Therefore, the AdS-SW voltammetric responses of 17.5 µM FVP and 9.5 µM PCT at bare GPE and Au@CCB/GNFPE were compared at pH 5.0 (Fig. S7). The GPE illustrates the poor oxidation peak currents of PCT (2.3 µA), and FVP (1.5 µA) (curve b). Fascinatingly, the Au@CCB/GNFPE sensor displays significantly higher oxidation peak currents for PCT (8.6 µA) and FVP (8.8 µA) (curve c) and lower oxidation potentials compared to bare GPE. All these results confirm that the Au@CCB/GNFPE acts as a good electro-catalyst for sensing the target analytes and this sensor is used for further studies.

Simultaneous electrochemical sensing of FVP and PCT in their binary mixture has been carried out at the Au@CCB/GNFPE sensor. Two well-defined AdS-SWV oxidation peaks could be observed at 470 mV for PCT and at 1050 mV for FVP in PB solution (Fig. 5A). Fig. 5B and 5C show the linear fits of FVP and PCT, and the corresponding linear functions can be deduced as:

$$I_{Pa}(\mu A) = 475\ C_{FVP}/\text{nmol L}^{-1} - 0.59\ (0.03–75.0\ \mu M)\ (R^2 = 0.9971);$$

$$I_{Pa}(\mu A) = 830\ C_{PCT}/\text{nmol L}^{-1} + 0.45\ (0.05–50.0\ \mu M)\ (R^2 = 0.9989)$$

The values of LOD and LOQ were cited in Table S1. The sensitivity of the sensing electrode toward the determination of PCT and FVP was observed to be 11.8 and 6.8 $\mu A \mu M^{-1}\ cm^{-2}$, respectively. The performance of the Au@CCB/GNFPE sensor in comparison with other published platforms for the detection of PCT [39–44] and FVP is shown in Table 3. The proposed sensor exhibited a broad linear range and lower detection limits for both the antiviral drug FVP and the co-administered drug PCT when compared with previously reported values. Thus, the present results confirmed the suitability of Au@CCB nanocomposite modified GNFPE as an attractive electro-catalytic platform for the simultaneous detection of FVP and PCT sensing in real samples.

3.10. Real sample analysis

3.10.1. Simultaneous analysis of FVP and PCT in plasma sample and dosage forms

To evaluate the practical performance, the Au@CCB/GNFPE was

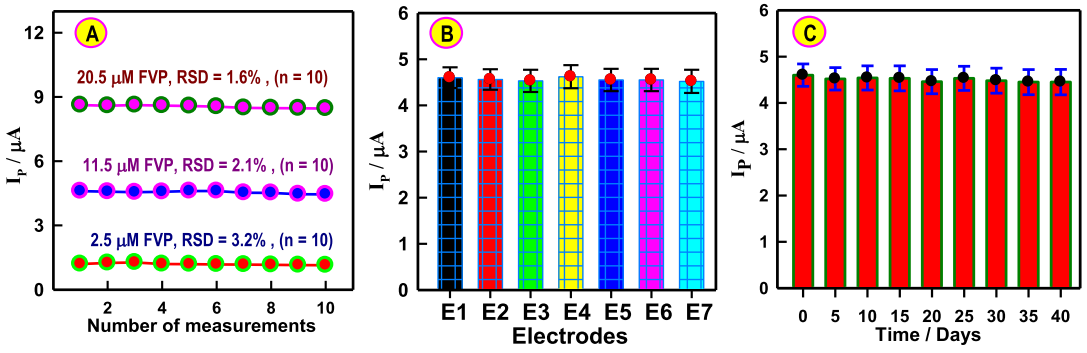

Fig. 4. (A) The repeatability of FVP determination with the Au@CCB/GNFPE sensor was evaluated from the peak current responses of ten measurements of FVP at concentrations of 2.5, 11.5 and 20.5 μM. (B) Reproducibility studies of seven different Au@CCB/GNFPE sensors for 11.5 μM FVP. (C) Long-term stability of Au@CCB/GNFPE sensor over 40 days.

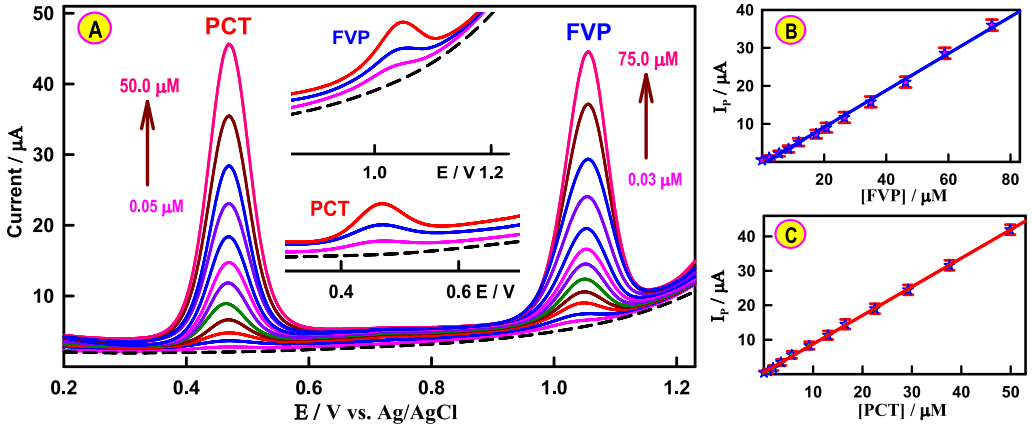

Fig. 5. (A) AdS-SW voltammograms of simultaneous determination of FVP (0.03 –75.0 μM) and PCT (0.05 – 50.0 μM) at Au@CCB/GNFPE in PB solution (pH 5.0). (B, C) Corresponding calibration plots for FVP and PCT. Error bar represents the standard deviation of triple measurements.

utilized for simultaneous analysis of FVP and PCT in spiked human plasma samples and in commercial tablets. The plasma samples were injected with known amounts of FVP and PCT, respectively, and subjected to AdS-SWV (Fig. S8A). As can be observed from Fig. S8B and C, peak current responses of both FVP and PCT exhibit strong linear relationships with increasing FVP and PCT concentrations. The linear working range and LOD were 0.04 – 75.0 μM and 7.3 nM for FVP and 0.03 – 51.0 μM and 4.0 nM for PCT, respectively (Table S2). As presented in Table 4, the recovery tests for FVP and PCT spiked samples were between 98.9% and 100.8%, with low RSDs (<2.3%). Moreover, the proposed AdS-SWV technique was applied for the sensing of FVP and PCT in dosage forms (Avipiravir 200 mg, Panadol 500 mg) using the electrochemical Au@CCB/GNFPE sensor (Fig. S9). To verify the applicability of the suggested AdS-SWV technique, the recovery rates were assessed and are depicted in Table 5. Based on these results, the constructed electrochemical Au@CCB/GNFPE sensor can be used to accurately detect FVP and PCT simultaneously in real samples.

Table 4
Recovery of FVP and PCT in human plasma samples (n = 3).

Compound	Spiked (μM)	Found (μM)	Precision RSD %	Recovery %
FVP	8.5	8.41	1.4	98.9
	17.5	17.57	1.6	100.4
	27.5	27.35	2.1	99.45
PCT	3.6	3.52	1.5	97.8
	13.5	13.45	1.9	99.60
	24.5	24.70	2.3	100.8

Table 5
Analysis of FVP and PCT in its commercial tablets by AdS-SWV using Au@CCB/GNFPE.

Sample	Spiked (μM)	Found[a] (μM)	RSD (%)	Recovery (%)
Avipiravir 200 mg	0.0	13.5	1.8	–
	12.0	25.22	2.2	98.9
	28.0	41.13	1.9	99.1
	46.5	61.30	2.5	102.2
Panadol 500 mg	0.0	9.3	2.3	–
	9.2	18.7	2.7	101.1
	18	26.8	1.6	98.2
	29.2	39.2	2.2	101.8

[a] Average of five determinations at optimum conditions.

3.10.2. *Simultaneous analysis of FVP and PCT in presence of AA*

The efficacy of the Au@CCB/GNFPE sensor was checked for the simultaneous analysis of FVP and PCT in the presence of some vital interfering drug AA, which may have a number of immune-modulatory mechanisms that can help to mitigate or reduce COVID-19 pathophysiology [45,46]. Therefore, simultaneous electrochemical sensing of FVP and PCT in plasma sample has been carried out at Au@CCB/GNFPE in the presence of AA. Fig. 6A displayed the AdS-SWV responses of various concentrations of FVP and PCT spiked plasma sample in presence of 100 μM AA. In the range of 0.04 – 76.0 μM, the peak current of FVP and its concentration exhibited good linearity, and the linear equation was $I_{Pa}(\mu A) = 485\ C_{FVP}/\text{nmol L}^{-1} - 0.58$, $R^2 = 0.9971$ (Fig. 6B), with LOD of 7.5 nM. Similarly, as can be seen in Fig. 6C, a linear equation $I_{pa}(\mu A) = 800\ C_{PCT}/\text{nmol L}^{-1} + 0.64$ ($R^2 = 0.9995$) of PCT was obtained with its

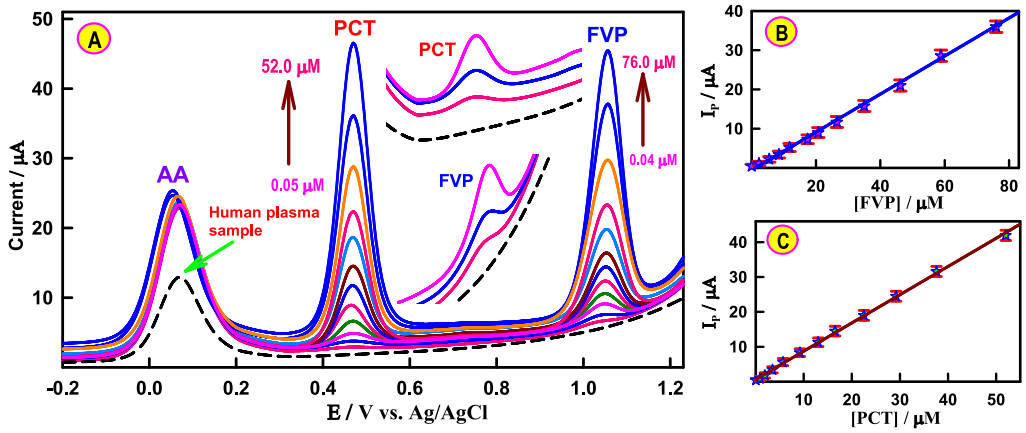

Fig. 6. (A) AdS-SW voltammograms of simultaneous determination of FVP (0.04 – 76.0 µM) and PCT (0.05 – 52.0 µM) spiked human plasma sample in presence of 100 µM AA at Au@CCB/GNFPE in PB solution (pH 5.0). (B, C) Corresponding calibration plots for FVP and PCT. Error bar represents the standard deviation of triple measurements.

concentration from 0.05 to 52.0 µM, and the LOD was 4.5 nM (Table S2). It is interesting to observe that the sensitivities of the Au@CCB/GNFPE towards the simultaneous analysis of FVP and PCT in the absence and presence of AA were virtually the same, which proved its potential sensing for simultaneous detection of these two drugs in real sample.

4. Conclusions

In this investigation, a new electrode material of gold nanoparticles anchored conductive carbon black (Au@CCB) was synthesized. The Au@CCB nanocomposite was characterized by TEM and EDX methods. The Au@CCB nanocomposite was used to modify GNFPE for an electrochemical sensing platform to determine the antiviral drug FVP in the absence and presence of the co-administered drug paracetamol (PCT). The constructed sensor has been shown to be a simple and highly effective platform for FVP oxidation with excellent sensitivity and increased selectivity even in the presence of common biological interfering analytes. In addition, the performance of the Au@CCB/GNFPE for the simultaneous detection of FVP and PCT was monitored. The LOD and LOQ were estimated to be 7.5 and 25.0 nM for FVP and 4.3 and 14.0 nM for PCT, respectively, at the Au@CCB/GNFPE. Moreover, the sensing electrode was efficiently applied to quantify the FVP and PCT in pharmaceuticals and plasma samples and obtained satisfactory recovery between 98.2 and 101.8% and 98.9–100.8%, respectively. Most importantly, the Au@CCB/GNFPE can be applied to determine FVP and PCT simultaneously in the presence of AA in plasma samples.

CRediT authorship contribution statement

Rasha M.K. Mohamed: Conceptualization, Funding acquisition, Investigation, Methodology, Project administration, Resources, Validation, Writing – review & editing. **Sabrein H. Mohamed:** Conceptualization, Funding acquisition, Investigation, Methodology, Project administration, Resources, Validation, Writing – review & editing. **Aml M. Asran:** Conceptualization, Funding acquisition, Investigation, Methodology, Project administration, Resources, Validation, Writing – review & editing. **Ibrahim H. Alsohaimi:** Conceptualization, Investigation, Methodology, Resources, Validation, Writing – review & editing. **Hassan M.A. Hassan:** Conceptualization, Investigation, Methodology, Resources, Validation, Writing – review & editing. **Hossieny Ibrahim:** Conceptualization, Data curation, Formal analysis, Investigation, Methodology, Software, Supervision, Validation, Visualization, Writing – original draft, Writing – review & editing. **Mohamed M. El-Wekil:** Conceptualization, Data curation, Formal analysis, Investigation, Methodology, Software, Supervision, Validation, Visualization, Writing – original draft, Writing – review & editing.

Declaration of Competing Interest

The authors declare that they have no known competing financial interests or personal relationships that could have appeared to influence the work reported in this paper.

Data availability

Data will be made available on request.

Acknowledgement

This work was funded by the Deanship of Scientific Research at Jouf University under Grant Number (DSR2022-RG-0135).

Appendix A. Supplementary data

Supplementary data to this article can be found online at https://doi.org/10.1016/j.microc.2023.108696.

References

[1] H.M. Dabbous, S. Abd-Elsalam, M.H. El-Sayed, A.F. Sherief, F.F.S. Ebeid, M.S.A. El Ghafar, S. Soliman, M. Elbahnasawy, R. Badawi, M.A. Tageldin, Efficacy of favipiravir in COVID-19 treatment: a multi-center randomized study, Arch. Virol. 166 (2021) 949–954.
[2] S. Joshi, J. Parkar, A. Ansari, A. Vora, D. Talwar, M. Tiwaskar, S. Patil, H. Barkate, Role of favipiravir in the treatment of COVID-19, Int. J. Infect. Dis. 102 (2021) 501–508.
[3] K. Habler, M. Brugel, D. Teupser, U. Liebchen, C. Scharf, U. Schonermarck, M. Vogeser, M. Paal, Simultaneous quantification of seven repurposed COVID-19 drugs remdesivir (plus metabolite GS-441524), chloroquine, hydroxychloroquine, lopinavir, ritonavir, favipiravir and azithromycin by a two-dimensional isotope dilution LC-MS/MS method in human serum, J. Pharm. Biomed. Anal. 196 (2021), 113935.
[4] S.M. Megahed, A.A. Habib, S.F. Hammad, A.H. Kamal, Experimental design approach for development of spectrofluorimetric method for determination of favipiravir; a potential therapeutic agent against COVID-19 virus: Application to spiked human plasma, Spectrochimica Acta Part A: Mol. Biomolecul. Spectrosc. 249 (2021) 119241.
[5] I.E. Mikhail, H. Elmansi, F. Belal, A. Ehab Ibrahim, Green micellar solvent-free HPLC and spectrofluorimetric determination of favipiravir as one of COVID-19 antiviral regimens, Microchem. J. 165 (2021), 106189.
[6] İ. Bulduk, HPLC-UV method for quantification of favipiravir in pharmaceutical formulations, Acta Chromatogr 33 (2021) 209–215.
[7] M. El-Awady, H. Elmansi, F. Belal, R. abo Shabana, Insights on the quantitative concurrent fluorescence-based analysis of Anti-COVID-19 drugs remdesivir and favipiravir, J. Fluorescence 32 (2022) 1941–1948.
[8] D.A.M. Noureldeen, J.M. Boushra, A.S. Lashien, A.F. Abdel Hakiem, T.Z. Attia, Novel environment friendly TLC-densitometric method for the determination of

anti-coronavirus drugs "Remdesivir and Favipiravir": Green assessment with application to pharmaceutical formulations and human plasma, Microchem. J. 174 (2022), 107101.
[9] K. Habler, M. Brügel, D. Teupser, U. Liebchen, C. Scharf, U. Schönermarck, M. Vogeser, M. Paal, Simultaneous quantification of seven repurposed COVID-19 drugs remdesivir (plus metabolite GS-441524), chloroquine, hydroxychloroquine, lopinavir, ritonavir, favipiravir and azithromycin by a two-dimensional isotope dilution LC–MS/MS method in human serum, J. Pharm. Biomed. Anal. 196 (2021), 113935.
[10] S. Allahverdiyeva, O. Yunusoğlu, Y. Yardım, Z. S¸entürk, First electrochemical evaluation of favipiravir used as an antiviral option in the treatment of COVID-19: a study of its enhanced voltammetric determination in cationic surfactant media using a boron-doped diamond electrode, Anal. Chim. Acta 1159 (2021), 338418.
[11] M.A. Mohamed, G.M.G. Eldin, S.M. Ismail, N. Zine, A. Elaissari, N. Jaffrezic Renault, A. Errachid, Innovative electrochemical sensor for the precise determination of the new antiviral COVID-19 treatment Favipiravir in the presence of coadministered drugs, J. Electroanal. Chem. 895 (2021) 115422.
[12] Ç. Kanbeş Dindar, B. Bozal-Palabiyik, B. Uslu, Development of a diamond nanoparticles-based nanosensor for detection and determination of antiviral drug favipiravir, Electroanalysis 34 (7) (2022) 1174–1186.
[13] A. Galal, Y.M. Ahmed, M.H.M. Ahmed, N.F. Atta, Electrochemistry and determination of an antiviral drug at ionic liquids crystals-carbon nanotubes modified glassy carbon electrode, J. Electrochem. Soc. 168 (2021), 116512.
[14] W. Bouali, N. Erk, G. Kholafazadehastamal, M. Naser, G. Tiris, Low-cost voltammetric sensor based on reduced graphene oxide anchored on platinum nanoparticles for robust determination of Favipiravir in real samples, Diamond Related Mater. 131 (2023), 109609.
[15] M.M. El-Wekil, A.M. Hayallah, M.A. Abdelgawad, M.A.S. Abourehab, R.Y. Shahin, Nanocomposite of gold nanoparticles@nickel disulfide-plant derived carbon for molecularly imprinted electrochemical determination of favipiravir, J. Electroanal. Chem. 922 (2022), 116745.
[16] N. Erk, M. Mehmandoust, M. Soylak, Electrochemical sensing of favipiravir with an innovative water-dispersible molecularly imprinted polymer based on the bimetallic metal-organic framework: comparison of morphological effects, Biosensors 12 (2022) 769.
[17] H. Ibrahim, Y. Temerk, Synergistic electrocatalytic activity of In_2O_3@FMWCNTs nanocomposite for electrochemical quantification of dobutamine in clinical patient blood and in injection dosage form, Talanta 208 (2020), 120362.
[18] H. Ibrahim, Y. Temerk, N. Farhan, A novel sensor based on nanobiocomposite Au-In_2O_3-chitosan modified acetylene black paste electrode for sensitive detection of antimycotic ciclopirox olamine, Talanta 179 (2018) 75–85.
[19] H. Ibrahim, M. Ibrahim, Y. Temerk, A novel megestrol acetate electrochemical sensor based on conducting functionalized acetylene black–CeO_2NPs nanohybrids decorated glassy carbon microspheres, Talanta 200 (2019) 324–332.
[20] H. Ibrahim, Y. Temerk, Gold nanoparticles anchored graphitized carbon nanofibers ionic liquid electrode for ultrasensitive and selective electrochemical sensing of anticancer drug irinotecan, Microchim. Acta 187 (2020) 579.
[21] H.M. Ali, I.H. Alsohaimi, A.A. Nayl, A.A. Essawy, M. Gamal, H. Ibrahim, A new ultrasensitive platform based on f-GCNFs@nano-CeO_2 core-shell nanocomposite for electrochemical sensing of oxidative stress biomarker 3-nitrotyrosine in presence of uric acid and tyrosine, Microchem. J. 183 (2022), 108068.
[22] F. Arduini, S. Cinti, V. Mazzaracchio, V. Scognamiglio, A. Amine, D. Moscone, Carbon black as an outstanding and affordable nanomaterial for electrochemical (bio)sensor design, Biosens. Bioelectron 156 (2020), 112033.
[23] T.A. Silva, F.C. Moraes, B.C. Janegitz, O. Fatibello-Filho, Electrochemical biosensors based on nanostructured carbon black: a review, J. Nanomater. 2017 (2017) 4571614.
[24] V. Mazzaracchio, M.R. Tomei, I. Cacciotti, A. Chiodoni, C. Novara, M. Castellino, G. Scordo, A. Amine, D. Moscone, F. Arduini, Inside the different types of carbon black as nanomodifiers for screen-printed electrodes, Electrochim. Acta 317 (2019) 673–683.
[25] R. Shanmugam, J. Ganesamurthi, T.-W. Chen, S.-M. Chen, M. Balamurugan, M. A. Ali, A.M. Al-Mohaimeed, W.A. Al-onazi, K. Alagumalai, Preparation and fabrication of porous-Fe_2O_3/carbon black nanocomposite: a portable electrochemical sensor for psychotropic drug detection in environmental samples, Mater. Today Chem. 25 (2022), 100982.
[26] Y. Liu, H. Li, S. Gong, Y. Chen, R. Xie, Q. Wu, J. Tao, F. Meng, P. Zhao, A novel nonenzymatic electrochemical biosensor based on the nanohybrid of bimetallic PdCu nanoparticles/carbon black for highly sensitive detection of H_2O_2 released from living cells, Sensors and Actuators, B: Chem. 290 (2019) 249–257.
[27] A. Wong, A. Martin Santos, T. Almeida Silva, O. Fatibello-Filho, Simultaneous determination of isoproterenol, acetaminophen, folic acid, propranolol and caffeine using a sensor platform based on carbon black, graphene oxide, copper nanoparticles and PEDOT: PSS, Talanta 1831 (2018) 329–338.
[28] J.A. Rather, A. Al Abri, P. Kannan, Electrochemical sensing of parabens in solubilized ionic liquid system at polyaniline decorated gold nanoparticles constructed interface, Microchem. J. 159 (2020), 105379.
[29] H. Ibrahim, Y. Temerk, A novel electrochemical sensor based on gold nanoparticles decorated functionalized carbon nanofibers for selective determination of xanthine oxidase inhibitor febuxostat in plasma of patients with gout, Sensors and Actuators: B. Chemical 347 (2021), 130626.
[30] M. Ibrahim, H. Ibrahim, N.B. Almandil, A. Kawde, A novel nanocomposite based on gold nanoparticles loaded on acetylene black for electrochemical sensing of the anticancer drug topotecan in the presence of high concentration of uric acid, J. Electroanal. Chem. 824 (2018) 22–31.
[31] J. Micallef, T. Soeiro, A.P. Jonville-Béra, COVID-19 and NSAIDs: primum non nocere, Therapies 75 (2020) 514.
[32] J.L.G. Fuente, M.V. Martínez-Huerta, S. Rojas, P. Terreros, J.L.G. Fierro, M.A. Peña, Methanol electrooxidation on PtRu nanoparticles supported on functionalized carbon black, Catal. Today 116 (2006) 422–432.
[33] H. Zhao, L. Dou, J. Ren, M. Cui, N. Li, X. Ji, X. Liu, C. Zhang, MOF-derived porous Co_3O_4 coupled with AuNPs and nucleic acids as electrocatalysis signal probe for sensitive electrochemical aptasensing of adenosine triphosphate, Sensors & Actuators: B. Chemical 362 (2022), 131753.
[34] G. Veerappan, K. Bojan, S.W. Rhee, Sub-micrometer-sized graphite as a conducting and catalytic counter electrode for dyesensitized solar cells, ACS Appl. Mater. Interfaces 3 (2011) 857–862.
[35] S. Shankar, N.S.K. Gowthaman, S.A. John, Synthesis of albumin capped gold nanoparticles and their direct attachment on glassy carbon electrode for the determination of nitrite ion, J. Electroanal. Chem. 828 (2018) 33–40.
[36] H. Ibrahim, Y. Temerk, A novel electrochemical sensor based on functionalized glassy carbon microparticles@CeO_2 core–shell for ultrasensitive detection of breast anticancer drug exemestane in patient plasma and pharmaceutical dosage form, Microchem. J. 167 (2021), 106264.
[37] H. Ibrahim, Y. Temerk, A novel disposable electrochemical sensor based on modifying graphite pencil lead electrode surface with nanoacetylene black for simultaneous determination of antiandrogens flutamide and cyproterone acetate, J. Electroanal. Chem. 859 (2020), 113836.
[38] S. Kubendhiran, R. Sakthivel, S.M. Chen, R. Anbazhagan, H.C. Tsai, A novel design and synthesis of ruthenium sulfide decorated activated graphite nanocomposite for the electrochemical determination of antipsychotic drug chlorpromazine, Compos. Part B-Eng. 168 (2018) 282–290.
[39] W. Si, W.u. Lei, Z. Han, Y. Zhang, Q. Hao, M. Xia, Electrochemical sensing of acetaminophen based on poly (3, 4-ethylenedioxythiophene)/graphene oxide composites, Sens. Actuators B 193 (2014) 823–829.
[40] N. Adhoum, L. Monser, M. Toumi, K. Boujlel, Determination of naproxen in pharmaceuticals by differential pulse voltammetry at a platinum electrode, Anal. Chim. Acta 495 (1–2) (2003) 69–75.
[41] N.S. Anuar, W.J. Basirun, M. Ladan, M.d. Shalauddin, M.S. Mehmood, Fabrication of platinum nitrogen-doped graphene nanocomposite modified electrode for the electrochemical detection of acetaminophen, Sens. Actuators B 266 (2018) 375–383.
[42] M.A. Hefnawy, S.S. Medany, S.A. Fadlallah, R.M. El-Sherif, S.S. Hassan, Novel self-assembly Pd(II)-schiff base complex modified glassy carbon electrode for electrochemical detection of paracetamol, Electrocatalysis 13 (5) (2022) 598–610.
[43] X.-Q. Cai, K. Zhu, B.-T. Liu, Q.-Y. Zhang, Y.-H. Luo, D.-E. Zhang, γ-Fe_2O_3/CNTs composites for electrochemical detection of paracetamol: synthesis, phase transition and enhanced properties, J. Electrochem. Soc. 168 (2021), 057511.
[44] M. Kumar, B.E.K. Swamy, S. Reddy, W. Zhao, S. Chetana, V.G. Kumar, ZnO/functionalized MWCNT and Ag/functionalized MWCNT modified carbon paste electrodes for the determination of dopamine, paracetamol and folic acid, J. Electroanal. Chem. 835 (2019) 96–105.
[45] G.P. Milani, M. Macchi, A. Guz-Mark, Vitamin C in the treatment of COVID-19, Nutrients 13 (2021) 1172.
[46] M.O. Yaseen, H. Jamshaid, A. Saif, T. Hussain, Immunomodulatory role and potential utility of various nutrients and dietary components in SARS-CoV-2 infection, Int. J. Vitam. Nutr. Res. 92 (2022) 35–48.